J|A|C|S

A R T I C L E S

Layer-by-Layer Assembly and Spontaneous Flocculation of Oppositely Charged Oxide and Hydroxide Nanosheets into Inorganic Sandwich Layered Materials

Liang Li, Renzhi Ma, Yasuo Ebina, Katsutoshi Fukuda, Kazunori Takada, and Takayoshi Sasaki*

Contribution from the Nanoscale Materials Center, National Institute for Materials Science, 1-1 Namiki, Tsukuba, Ibaraki 305-0044, Japan

Received March 19, 2007; E-mail: sasaki.takayoshi@nims.go.jp

Abstract: Exfoliated oxide nanosheets such as $Ti_{0.91}O_2$ and $Ca_2Nb_3O_{10}$ and layered double hydroxide (LDH) nanosheets of $Mg_{2/3}Al_{1/3}(OH)_2$ were restacked into inorganic sandwich layered materials. Sequential adsorption of these oppositely charged nanosheets from their colloidal suspensions yielded multilayer ultrathin films while their simple mixing produced lamellar flocculates. Eliminating carbonate ions from the reaction system was found to be essential for successfully achieving the sandwich structures. The flocculated materials as well as the films were characterized by atomic force microscopy (AFM), UV−visible absorption spectroscopy, X-ray photoelectron spectroscopy, X-ray diffraction (XRD), transmission electron microscopy (TEM), and chemical analysis, which all supported the formation of the ordered sandwich structures. AFM observations revealed alternate dense tiling of LDH nanosheets and oxide nanosheets onto a substrate surface. UV−visible absorption spectra exhibited progressive enhancement of optical density due to oxide nanosheets as a function of deposition cycles, providing strong evidence for regular growth of multilayer films. The combinations of $Mg_{2/3}Al_{1/3}(OH)_2/Ti_{0.91}O_2$ and $Mg_{2/3}Al_{1/3}(OH)_2/Ca_2Nb_3O_{10}$ produced XRD Bragg peaks having multilayer spacings of 1.2 and 2.0 nm, respectively. These basal spacing values are compatible with the sum of thickness of LDH nanosheets and corresponding oxide nanosheets. TEM images of flocculated samples displayed lamellar features with two different constituent layers appearing alternately.

Introduction

A very large number of inorganic layered compounds having ion-exchange properties are known and have been extensively investigated from various standpoints.[1−5] Thanks to the ion-exchange reactivities, a range of foreign species can be regularly inserted into interlayer galleries, yielding a diverse range of nanocomposites. A drastic change in physical properties has often been achieved in these processes. One of the hot topics in layered materials is their delamination into colloidal single layers.[6,7] Resulting nanosheets can be taken as a class of two-dimensional nanoscale materials. They are found to exhibit peculiar physical and chemical properties associated with their thickness at a nanometer range.

Ion-exchangeable layered compounds can be classified into two groups depending on the reactivities that they show: cation-exchange or anion-exchange properties. The compounds in the former group are composed of negatively charged host layers and charge-balancing interlayer cations. Delamination has been reported for various layered compounds belonging to this group: smectite clay minerals;[8] transition metal dichalcogenides[9] and oxides;[10−14] metal phosphates.[15] Particularly the successful delamination of layered perovskites,[10] layered titanates,[11] and layered manganese oxides[14] has triggered keen interest in

(1) *Inorganic Ion Exchange Materials*; Clearfield, A., Ed.; CRC Press, Inc.: Boca Raton, FL, 1982.
(2) *Intercalation Chemistry*; Whittingham, M. S., Jacobson, A. J., Eds.; Academic Press: New York, 1982.
(3) *Handbook of Layered Materials*; Auerbach, S. M., Carrado, K. A., Dutta, P. K., Eds.; Marcel Dekker, Inc.: New York, 2004.
(4) Clearfield, A. *Chem. Rev.* **1988**, *88*, 125.
(5) Ogawa, M.; Kuroda, K. *Chem. Rev.* **1995**, *95*, 399.
(6) Jacobson, A. J. *Comprehensive Supramolecular Chemistry*; Alberti, G., Bein, T., Eds.; Elsevier Science: Oxford, UK, 1996; Vol. 7, pp 315−335.
(7) Sasaki T. *Encyclopedia of Nanoscience and Nanotechnology*; Nalwa, H. S., Ed.; American Scientific Publishers: Stevenson Ranch, CA, 2002.
(8) (a) MacEwan, D. M. C.; Wilson, M. J. Interlayer and Intercalation Complexes of Clay Minerals. In *Crystal Structures of Clay Minerals and Their X-ray Identification*; Brindley, G. W., Brown, G., Eds.; Mineralogical Society: London, 1980. (b) Nadeau, P. H.; Wilson, M. J.; McHardy, W. J.; Tait, J. M. *Science* **1984**, *225*, 923. (c) Tamura, K.; Sasaki, T.; Yamada, H.; Nakazawa, H. *Langmuir* **1999**, *15*, 5509.
(9) (a) Murphy, D. W.; Hull, G. W., Jr. *J. Chem. Phys.* **1975**, *62*, 973. (b) Lerf, A.; Schöllhorn, R. *Inorg. Chem.* **1977**, *16*, 2950. (c) Joensen, P.; Frindt, R. F.; Morrison, S. R. *Mater. Res. Bull.* **1986**, *21*, 457. (d) Yang, D; Jiménez Sandoval, S.; Divigalpitiya, W. M. R.; Irwin, J. C.; Frindt, R. F. *Phys. Rev. B* **1991**, *43*, 12053. (e) Yang, D; Frindt, R. F. *J. Phys. Chem. Solids* **1996**, *57*, 1113.
(10) (a) Treacy, M. M. J.; Rice, S. B.; Jacobson, A. J.; Lewandowski, J. T. *Chem. Mater.* **1990**, *2*, 279. (b) Domen, K.; Ebina, Y.; Ikeda, S.; Tanaka, A.; Kondo, J. N.; Maruya, K. *Catal. Today* **1996**, *28*, 167. (c) Schaak, R. E.; Mallouk, T. E. *Chem. Mater.* **2000**, *12*, 3427 (d) Schaak, R. E.; Mallouk, T. E. *Chem. Mater.* **2002**, *14*, 1455. (e) Han, Y.-S.; Park, I.; Choy, J.-H. *J. Mater. Chem.* **2001**, *11*, 1277. (f) Ebina, Y.; Sasaki, T.; Watanabe, M. *Solid-State Ionics* **2002**, *151*, 177.
(11) (a) Sasaki, T.; Watanabe, M.; Hashizume, H.; Yamada, H.; Nakazawa, H. *J. Chem. Soc., Chem. Commun.* **1996**, 229. (b) Sasaki, T.; Watanabe, M.; Hashizume, H.; Yamada, H.; Nakazawa, H. *J. Am. Chem. Soc.* **1996**, *118*, 8329. (c) Sasaki, T.; Watanabe, M. *J. Am. Chem. Soc.* **1998**, *120*, 4682. (d) Tanaka, T.; Ebina, Y.; Takada, K.; Kurashima, K.; Sasaki, T. *Chem. Mater.* **2003**, *15*, 3564. (e) Sugimoto, W.; Tarabayashi, O.; Murakami, Y.; Takasu, Y. *J. Mater. Chem.* **2002**, *12*, 3814. (f) Miyamoto, N.; Kuroda, K.; Ogawa, M. *J. Mater. Chem.* **2004**, *14*, 165.

the nanosheets because of their attractive functionalities. These layered materials have been exfoliated into colloidal polyanionic nanosheets typically by intercalation of bulky guests such as quaternary ammonium ions.

On the other hand, compounds in the second group are relatively rare, and layered double hydroxides (LDHs) are the most well-studied among them. LDHs, known as hydro-talcite-like compounds, have a general chemical formula of $[M^{2+}_{1-x}M^{3+}_x(OH)_2][(A^{n-})_{x/n}\cdot mH_2O]$. The host layer is of brucite ($Mg(OH)_2$)-type, and partial substitution of divalent metal ions, M^{2+}, by trivalent ones, M^{3+}, yields the excessive positive charge, $+x$, which is compensated for by interlayer counteranions, A^{n-}, such as Cl^-, NO_3^-, SO_4^{2-}, and CO_3^{2-}. Much attention has been paid to delamination of LDHs, which should produce positively charged sheets in contrast to the majority of polyanionic nanosheets derived from cation-exchangeable layered materials. However, the successful synthesis of LDH nanosheets has been attained only recently.[16] We have reported that the action of formamide on LDHs in nitrate form can induce exfoliation into colloidal unilamellar sheets.[16e-h] Because this process can be applied to micrometer-sized crystals with well-developed hexagonal shape prepared by the so-called homogeneous precipitation, highly crystalline nanosheets of several micrometers in size could be obtained.

One of the most important and attractive aspects of the exfoliated nanosheets is that various nanostructures can be fabricated using them as two-dimensional building blocks.[17-19]

It is even possible to tailor superlattice-like assemblies, incorporating a wide range of materials, such as organic molecules, polymers, and inorganic and metal nanoparticles, into the nanosheet galleries.[17-19,20-23] Sophisticated functionalities or nanodevices may be designed through the selection of nanosheets and combining materials and precise control over their arrangements at a molecular scale.[24-26] However, direct assembly of positively and negatively charged nanosheets has not been achieved yet, although such sandwich lamellar systems are intriguing and may be one of the ultimate challenges for material syntheses with nanosheets. The process will provide a new and rational way to design new materials with a precisely controlled nanostructure.

In this work, we report the synthesis and characterizations of sandwich structured layered materials through direct combination of oppositely charged building blocks, i.e., positively charged LDH nanosheets ($Mg_{2/3}Al_{1/3}(OH)_2$) and negatively charged oxide nanosheets ($Ti_{0.91}O_2$ and $Ca_2Nb_3O_{10}$), the structure of which are schematically illustrated in Figure 1. The procedures for exfoliation into unilamellar sheets with a thickness of $0.48-1.44$ nm have been well-established, and thus, these nanosheets are suitable as model building blocks.[10,11,16] This work addresses the challenge to artificially organize these inorganic nanosheets into stacked superlattice-like systems through layer-by-layer assembly and flocculation. Heteroassembly of oppositely charged nanosheets at the molecular level has been accomplished.

Experimental Section

Reagents and Materials. Chemicals used were of reagent grade or higher purity. Milli-Q filtered water ($\rho > 17$ MΩ cm) was used throughout the experiments. The nanosheets were prepared according to delamination procedures described in our previous papers.[10f,11a-c,16e] Briefly, precursor layered metal oxides of $Cs_{0.7}Ti_{1.825}\square_{0.175}O_4$ ($\square$: vacancy) and $KCa_2Nb_3O_{10}$ were synthesized by solid-state calcination of a mixture of starting raw materials, such as alkali-metal carbonates, CaO, TiO_2, and Nb_2O_5, at 800 and 1100°C, respectively. They were converted into protonic oxides, $H_{0.7}Ti_{1.825}\square_{0.175}O_4\cdot H_2O$ and $HCa_2Nb_3O_{10}\cdot 1.5H_2O$, by repeating acid-exchange several times using a 1 M HCl solution. Next, 1 g of obtained protonic oxides was shaken with 250 cm^3 of an aqueous solution of $(C_4H_9)_4NOH$ for 10 days, which induced delamination into colloidal unilamellar nanosheets of $Ti_{0.91}O_2$ and $Ca_2Nb_3O_{10}$. The obtained aqueous suspensions were freeze-dried and then redispersed into formamide. The suspensions containing $0.4-0.5$ g of nanosheets were obtained after a small amount of nondispersed solid was removed by centrifugation at 3500 rpm. On the other hand, a well-crystallized LDH sample, $[Mg_{2/3}Al_{1/3}(OH)_2][(CO_3)_{1/6}\cdot 0.5H_2O]$, was synthesized by reacting a mixed solution of $Mg(NO_3)_2$, $Al(NO_3)_3$, and hexamethylenetetramine (2/1/5 in molar ratio) under hydrothermal conditions at 140 °C.[27] The obtained microcrystals (1 g) were reacted

(12) (a) Abe, R.; Shinohara, K.; Tanaka, A.; Hara, M.; Kondo, J. N.; Domen, K. *J. Mater. Res.* **1998**, *13*, 861. (b) Saupe, G. B.; Waraksa, C. C.; Kim, H.-N.; Han, Y. J.; Kaschak, D. M.; Skinner, D. M.; Mallouk, T. E. *Chem. Mater.* **2000**, *12*, 1556. (c) Miyamoto, N.; Nakato, T. *Adv. Mater.* **2002**, *14*, 1267. (d) Miyamoto, N.; Yamamoto, H.; Kaito, R.; Kuroda, K. *Chem. Commun.* **2002**, 2378. (e) Takagaki, A.; Lu, D.; Kondo, J. N.; Hara, M.; Hayashi, S.; Domen, K. *Chem. Mater.* **2005**, *17*, 2487.
(13) (a) Takagaki, A.; Sugisawa, M.; Lu, D.; Kondo, J. N.; Hara, M.; Domen, K.; Hayashi, S. *J. Am. Chem. Soc.* **2003**, *125*, 5479. (b) Takagaki, A.; Yoshida, T.; Lu, D.; Kondo, J. N.; Hara, M.; Domen, K.; Hayashi, S. *J. Phys. Chem. B* **2004**, *108*, 11549. (c) Du, G. H.; Yu, Y.; Chen, Q.; Wang, R. H.; Zhou, W.; Peng, L.-M. *Chem. Phys. Lett.* **2003**, *377*, 445.
(14) (a) Liu, Z.-H.; Ooi, K.; Kanoh, H.; Tang, W.-P.; Tomida, T. *Langmuir* **2000**, *16*, 4154. (b) Gao, Q.; Giraldo, O.; Tong, W.; Suib, S. L. *Chem. Mater.* **2001**, *13*, 778. (c) Omomo, Y.; Sasaki, T.; Wang, L. Z.; Watanabe, M. *J. Am. Chem. Soc.* **2003**, *125*, 3568. (d) Yang, X.; Makita, Y.; Liu, Z.-H.; Sakane, K.; Ooi, K. *Chem. Mater.* **2004**, *16*, 5581.
(15) (a) Alberti, G.; Casciola, M; Costantino, U. *J. Colloid Interface Sci.* **1985**, *107*, 256. (b) Alberti, G.; Giontella, E.; Murcia-Mascarós, S. *Inorg. Chem.* **1997**, *36*, 2844. (c) Alberti, G.; Cavalaglio, S.; Dionigi, C.; Marmottini, F. *Langmuir* **2000**, *16*, 7663. (d) Nakato, T.; Furumi, Y.; Terao, N.; Okuhara, T. *J. Mater. Chem.* **2000**, *10*, 737. (e) Yamamoto, N.; Okuhara, T.; Nakato, T. *J. Mater. Chem.* **2001**, *11*, 1858.
(16) (a) Adachi-Pagano, M.; Forano, C.; Besse, J.-P. *Chem. Commun.* **2000**, 91. (b) Leroux, F.; Adachi-Pagano, M.; Intissar, M.; Chauvière, S.; Forano, C.; Besse, J.-P. *J. Mater. Chem.* **2001**, *11*, 105. (c) Hibino, T.; Jones, W. *J. Mater. Chem.* **2001**, *11*, 1321. (d) Hibino, T. *Chem. Mater.* **2004**, *16*, 5482. (e) Li, L.; Ma, R.; Ebina, Y.; Iyi, N.; Sasaki, T. *Chem. Mater.* **2005**, *17*, 4386. (f) Liu, Z.; Ma, R.; Osada, M.; Iyi, N.; Ebina, Y.; Takada, K.; Sasaki, T. *J. Am. Chem. Soc.* **2006**, *128*, 4872. (g) Liu, Z.; Ma, R.; Ebina, Y.; Iyi, N.; Takada, K.; Sasaki, T. *Langmuir* **2007**, *23*, 861. (h) Ma, R.; Liu, Z.; Li, L.; Iyi, N.; Sasaki, T. *J. Mater. Chem.* **2006**, *16*, 3809. (i) Wu, Q.; Olafsen, A.; Vistad, Ø. B.; Roots, J.; Norby, P. *J. Mater. Chem.* **2005**, *15*, 4695. (j) Hibino, T.; Kobayashi, M. *J. Mater. Chem.* **2005**, *15*, 653.
(17) (a) Kleinfeld, E. R.; Ferguson, G. S. *Science* **1994**, *265*, 370. (b) Keller, S. W.; Kim, H.-N.; Mallouk, T. E. *J. Am. Chem. Soc.* **1994**, *116*, 8817. (c) Kim, H.-N.; Keller, S. W.; Mallouk, T. E.; Schmitt, J.; Decher, G. *Chem. Mater.* **1997**, *9*, 1414. (d) Fang, M.; Kim, C. H.; Saupe, G. B.; Kim, H.-N.; Waraksa, C. C.; Miwa, T.; Fujishima, A.; Mallouk, T. E. *Chem. Mater.* **1999**, *11*, 1526. (e) Schaak, R. E.; Mallouk, T. E. *Chem. Mater.* **2000**, *12*, 2513.
(18) (a) Sasaki, T.; Ebina, Y.; Watanabe, M.; Decher, G. *Chem. Commun.* **2000**, 2163. (b) Sasaki, T.; Ebina, Y.; Tanaka, T.; Harada, M.; Watanabe, M.; Decher, G. *Chem. Mater.* **2001**, *13*, 4661. (c) Wang, L. Z.; Omomo, Y.; Sakai, N.; Fukuda, K.; Nakai, I.; Ebina, Y.; Takada, K.; Watanabe, M.; Sasaki, T. *Chem. Mater.* **2003**, *15*, 2873. (d) Tanaka, T.; Fukuda, K.; Ebina, Y.; Takada, K.; Sasaki, T. *Adv. Mater.* **2004**, *16*, 872.
(19) (a) Muramatsu, M.; Akatsuka, K.; Ebina, Y.; Wang, K.; Sasaki, T.; Ishida, T.; Miyake, K.; Haga, M. *Langmuir* **2005**, *21*, 6590. (b) Umemura, Y.; Shinohara, E.; Koura, A.; Nishioka, T.; Sasaki, T. *Langmuir* **2006**, *22*, 3870.
(20) (a) Wang, L. Z.; Ebina, Y.; Takada, K.; Sasaki, T. *J. Phys. Chem. B* **2004**, *108*, 4283. (b) Wang, L. Z.; Sakai, N.; Ebina, Y.; Takada, K.; Sasaki, T. *Chem. Mater.* **2005**, *17*, 1352.
(21) Wang, Z.-S.; Ebina, Y.; Takada, K.; Watanabe, M.; Sasaki, T. *Langmuir* **2003**, *19*, 9534.
(22) Yui, T.; Tsuchino, T.; Itoh, T.; Ogawa, M.; Fukushima, Y.; Takagi, K. *Langmuir* **2005**, *21*, 2644.
(23) Zhou, Y.; Ma, R.; Ebina, Y.; Takada, K.; Sasaki, T. *Chem. Mater.* **2006**, *18*, 1235.
(24) Mallouk, T. E.; Gavin, J. A. *Acc. Chem. Res.* **1998**, *31*, 209.
(25) Kaschak, D. M.; Lean, J. T.; Waraksa, C. C.; Saupe, G. B.; Usami, H.; Mallouk, T. E. *J. Am. Chem. Soc.* **1999**, *121*, 3435.
(26) Osada, M.; Ebina, Y.; Takada, K.; Sasaki, T. *Adv. Mater.* **2006**, *18*, 295.
(27) (a) Iyi, N.; Matsumoto, T.; Kaneko, Y.; Kitamura, K. *Chem. Lett.* **2004**, *33*, 1122. (b) Iyi, N.; Matsumoto, T.; Kaneko, Y.; Kitamura, K. *Chem. Mater.* **2004**, *16*, 2926.
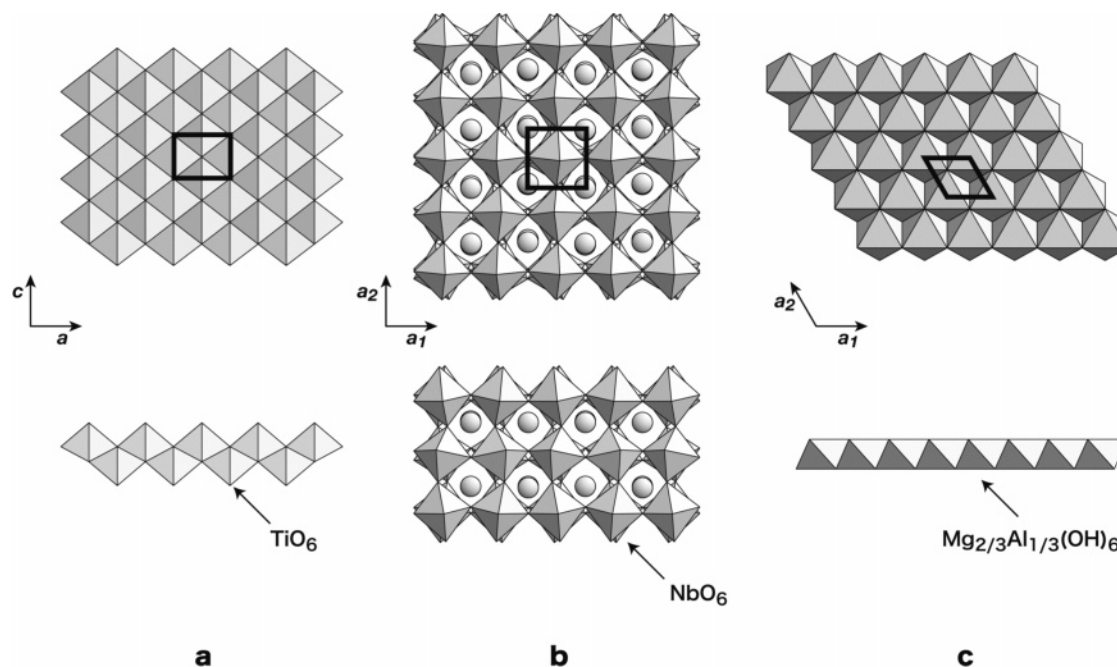
Figure 1. Top and side views of nanosheets: (a) $Ti_{0.91}O_2$; (b) $Ca_2Nb_3O_{10}$; (c) $Mg_{2/3}Al_{1/3}(OH)_2$. Two-dimensional unit cell indicated by thick lines is rectangular ($a = 0.3760(1)$ nm, $c = 0.2967(2)$ nm; $Z = 2$) for (a), square ($a = 0.3861(6)$ nm; $Z = 1$) for (b), and hexagonal ($a = 0.3038(2)$ nm; $Z = 1$) for (c). The sheets extend in a substantially infinite fashion on this scale.

with 1000 cm³ of a 1 M $NaNO_3$ aqueous solution containing 0.005 M HNO_3. The resulting LDH in nitrate form (1 g) was shaken in 1000 cm³ of formamide for 24 h to produce a colloidal suspension of exfoliated single layers.[16e]

Synthesis of Sandwich Layered Materials. All the experiments were carried out in a Schlenk bag, which was filled with N_2 gas to suppress the contamination of CO_2 from the air.

(a) Multilayer Films. Multilayer ultrathin films composed of LDH nanosheets and oxide nanosheets were fabricated by applying sequential adsorption procedure similar to that described in literature.[18] Substrates, such as a Si wafer chip and a quartz glass slide, were cleaned by treatment in a bath of methanol/HCl (1/1 in volume) and then concentrated H_2SO_4 for 20 min each. The substrate was first immersed in the formamide suspension of LDH nanosheets ($c = 0.5$ g dm⁻³) for 20 min, followed by thorough washing with formamide. Then the substrate was dipped into the formamide suspension of colloidal oxide nanosheets ($c = 0.2$ g dm⁻³) for 20 min and washed again. A series of these operations was repeated n times to obtain multilayer films of (LDH/oxide nanosheets)$_n$. The resulting film was dried under a N_2 gas stream.

(b) Flocculated Samples. Flocculated samples were prepared by slow addition of the formamide suspension of LDH nanosheets ($c = 0.5$ g dm⁻³) to the formamide suspension of colloidal oxide nanosheets ($c = 0.2$ g dm⁻³) under stirring at room temperature. A precipitated flocculate was separated by centrifuging at 3000 rpm, washed with formamide, and dried at 100 °C for 24 h.

Characterizations. X-ray diffraction (XRD) data were collected using a Rigaku Rint-2000 powder diffractometer with graphite mono-chromatized Cu Kα radiation ($\lambda = 0.154~05$ nm).

A Seiko SPS-1100 AFM instrument was employed to obtain a topographical image of the ultrathin films. Measurements were carried out in tapping mode with Si-tip cantilevers (force constant: 14 N·m⁻¹).

UV−visible absorption spectra for the multilayer films fabricated on a quartz glass substrate were recorded in a transmission mode using a Hitachi U-4000 spectrophotometer.

Transmission electron microscopy (TEM) observations were performed on a field emission JEM-3000F (JEOL) electron microscope operated at 300 kV equipped with a Gatan-666 electron energy loss spectrometer and energy dispersive X-ray spectrometer.

X-ray photoelectron spectra (XPS) were recorded on a Physical Electronics XPS-5700 spectrometer with Al Kα X-ray line (1486.6 eV). A depth profile was obtained by etching the films with Ar⁺ gun (3.0 kV).

A composition of the flocculated materials was determined by wet chemical analysis. Contents of Mg, Al, Ti, Ca, and Nb were determined by inductively coupled plasma (ICP) atomic emission spectroscopy (SEIKO SPS1700HVR) after decomposing the sample with a $K_2S_2O_7$ melt followed by dissolving with pure water. A carbon content was obtained by integrating the IR signal of CO_2 evolved in the heating process (LECO RC-412). Ignition loss was measured by heating at 1000 °C for 2 h.

Results and Discussion

Nanosheets as Building Components. The nanosheets synthesized were confirmed to be unilamellar and have lateral dimensions of 300−500 nm for $Ti_{0.91}O_2$ and $Ca_2Nb_3O_{10}$ and 2−3 μm for $Mg_{2/3}Al_{1/3}(OH)_2$ by AFM observations, which are comparable to those in our previous studies.[10f,11b,c,16e] The nanosheets, two-dimensional single crystals as illustrated in Figure 1, showed sharp diffraction lines in their in-plane XRD pattern (see Supporting Information, Figure S1). The patterns can be indexed based on two-dimensional rectangular, square, and hexagonal lattice for $Ti_{0.91}O_2$, $Ca_2Nb_3O_{10}$, and $Mg_{2/3}$-$Al_{1/3}(OH)_2$, respectively. Two-dimensional unit cell parameters were refined to be $a = 0.3760(1)$ nm, $c = 0.2967(2)$ nm for $Ti_{0.91}O_2$, $a = 0.3861(6)$ nm for $Ca_2Nb_3O_{10}$, and $a = 0.3038(2)$ nm for $Mg_{2/3}Al_{1/3}(OH)_2$. The thickness for $Ti_{0.91}O_2$ nanosheet has been determined as 0.73 nm by XAFS analysis in our previous study.[28] The thickness of the $Mg_{2/3}Al_{1/3}(OH)_2$ nanosheet is well-known as 0.48 nm.[29] On the other hand, literature data are not available for the $Ca_2Nb_3O_{10}$ nanosheet. However, the

(28) Fukuda, K.; Nakai, I.; Oishi, C.; Nomura, M.; Harada, M.; Ebina, Y.; Sasaki, T. *J. Phys. Chem. B* **2004**, *108*, 13088.
(29) Roy, A.; Forano, C.; Malki, K. E.; Besse, J.-P. *Anionic Clays: Trends in Pillaring Chemistry*; In *Synthesis of Microporous Materials*; Occelli, M. L., Robson, H. E., Eds.; Van Nostrand Reinhold: New York, 1992.
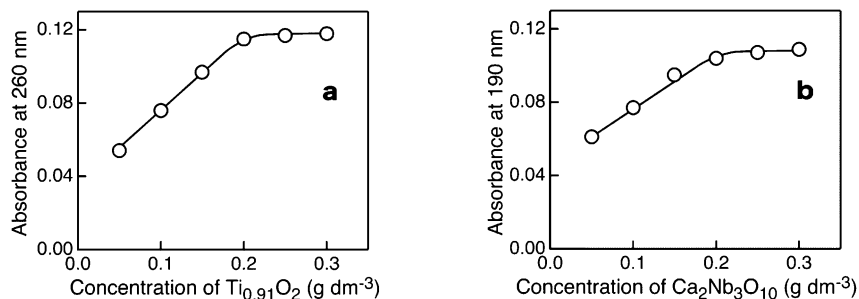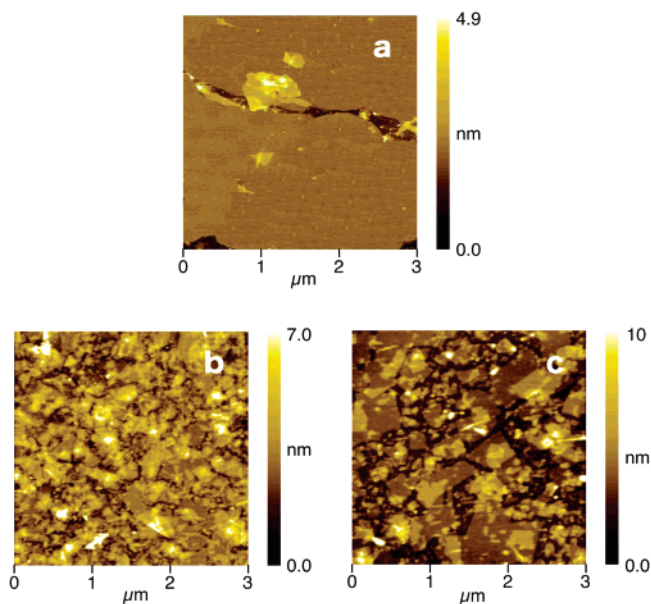
Figure 2. Absorbance of bilayer films as a function of concentration of oxide nanosheets: (a) $Mg_{2/3}Al_{1/3}(OH)_2/Ti_{0.91}O_2$; (b) $Mg_{2/3}Al_{1/3}(OH)_2/Ca_2Nb_3O_{10}$. The deposition time was fixed at 20 min.

thickness can be evaluated as 1.44 nm ($= 0.386 \times 3 + 0.14 \times 2$) because the sheet normal is composed of apex-shared three octahedra.[30] These structural parameters are very important to understand the inorganic sandwich structures composed of these LDH and oxide nanosheets, as will be described later.

The aqueous suspensions of oxide nanosheets, $Ti_{0.91}O_2$ and $Ca_2Nb_3O_{10}$, were converted into formamide ones. This procedure was necessary to attain stable interaction between LDH nanosheets and oxide nanosheets, suppressing the interference from CO_3^{2-} ions. The former sheets could not be well stabilized in aqueous media but only available as dispersion in formamide. The colloidal oxide nanosheets were obtained via the delamination of layered precursors in an aqueous alkaline solution of $(C_4H_9)_4NOH$, which inevitably absorbed a significant amount of CO_2 from the air to produce CO_3^{2-} ions. It is known that CO_3^{2-} ions have a very strong affinity to LDH.[29] In practice, when LDH and oxide nanosheets were interacted without special caution, self-restacking of LDH sheets accommodating CO_3^{2-} ions was dominating.[31] In this study, a freeze-drying method was employed to prepare a dried sample of oxide nanosheets from their aqueous suspensions, which was proved effective for removal of CO_3^{2-} ions from the reaction system. The freeze-dried woollike samples were mainly composed of oxide nanosheets and $(C_4H_9)_4N^+$ ions. Stable colloidal suspensions, substantially free from carbonate ions, were obtained by redispersing the dried samples in formamide and used as a source of oxide nanosheets in all preparations.

Layer-by-Layer Assembly of LDH Nanosheets and Oxide Nanosheets. Fabrication of self-assembled multilayer films with a sandwich structure could be initiated by treating a substrate with colloidal LDH nanosheets, followed by normal alternate adsorption of oxide nanosheets and LDH nanosheets. The direct coating of LDH nanosheets on a bare substrate surface was demonstrated in our previous reports.[16e,f]

There are several deposition parameters to be optimized in preparation of a high-quality film of nanosheets. Generally, the concentration of adsorbing species and its deposition duration are two important factors. Because conditions for monolayer deposition of LDH nanosheets have been established in previous work,[16e,f] such typical deposition parameters (sol concentration, 0.5 g dm^{-3}; deposition time, 20 min) were used in this study. As to oxide nanosheets, this is the first time using formamide

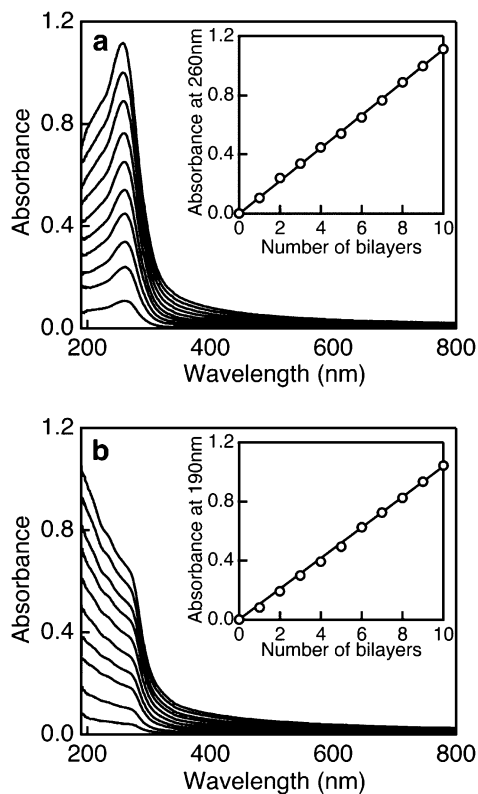(30) A height of one octahedron is 0.386 nm, and a double of the ionic radii for oxygen (0.14 nm) on both sides of the sheet should be added.

(31) When the as-prepared aqueous suspensions of oxide nanosheets were employed, a basal diffraction peak due to LDH in carbonate form was dominantly strong in comparison with those from a stacked structure of LDH/oxide sheets. The aqueous suspensions have high pH values (>11) and naturally contain CO_3^{2-} ions from the air.

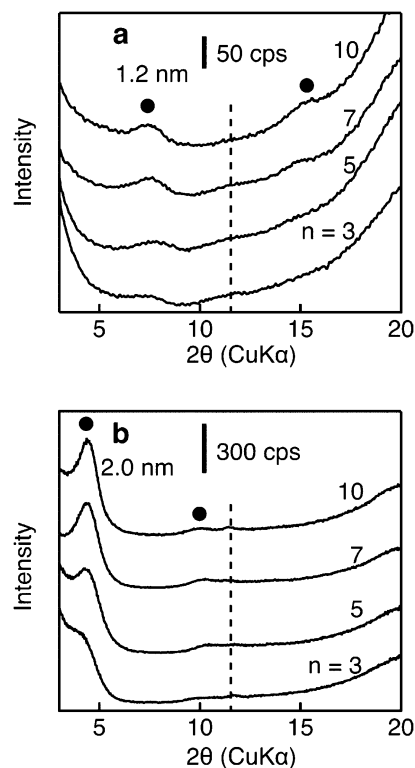**Figure 3.** Tapping-mode AFM images: (a) first layer of $Mg_{2/3}Al_{1/3}(OH)_2$ nanosheets deposited on an Si wafer and the subsequent layer of oxide nanosheets; (b) $Ti_{0.91}O_2$ nansheets; (c) $Ca_2Nb_3O_{10}$ nanosheets. In (a), two sheets as large as several micrometers are seen having a gap between them. On the other hand, many oxide nanosheets with a lateral size of several hundred nanometers cover the surface in (b) and (c).

suspensions in the layer-by-layer assembly, and suitable deposition conditions were explored. Figure 2 shows optical absorbance of bilayer films of LDH/oxide nanosheets deposited on a quartz glass substrate as a function of the concentration of oxide nanosheets. The absorption at 260 and 190 nm is characteristic of $Ti_{0.91}O_2$ and $Ca_2Nb_3O_{10}$ nanosheets, respectively. The absorbance, which is proportional to an adsorbed amount of oxide nanosheets, tended to increase with the concentration up to 0.2 g dm^{-3}. There was no obvious increment above this concentration, suggesting a saturation of adsorption. Similarly the absorbance was found to become constant for deposition times of 20 min and longer. Thus, we employed the nanosheet concentration of 0.2 g dm^{-3} and duration of 20 min as the optimum deposition parameters.

AFM images shown in Figure 3 display the surface topography of the first deposited layer of LDH nanosheets on the Si wafer and a subsequent layer of oxide nanosheets on top of it. The surface was densely covered with LDH nanosheet crystallites of several micrometers in lateral size after the first-layer deposition (Figure 3a). The thickness of the two-dimensional crystallites was measured to be about 0.8 nm, confirming that unilamellar LDH nanosheets were adsorbed. The monolayer region of the LDH nanosheets was predominant, although some

Figure 4. UV−visible absorption spectra of the multilayer films of (a) $(Mg_{2/3}Al_{1/3}(OH)_2/Ti_{0.91}O_2)_n$ and (b) $(Mg_{2/3}Al_{1/3}(OH)_2/Ca_2Nb_3O_{10})_n$ fabricated on a quartz glass substrate.


Figure 5. XRD patterns of as-prepared multilayer thin films of (a) $(Mg_{2/3}Al_{1/3}(OH)_2/Ti_{0.91}O_2)_n$ and (b) $(Mg_{2/3}Al_{1/3}(OH)_2/Ca_2Nb_3O_{10})_n$. Circles denote diffraction peaks from the sandwich structure. A broken line indicates the position of the first basal peak from LDH in carbonate form ($d = 0.76$ nm). A tilted baseline toward 20° in 2θ is due to an amorphous halo from a quartz glass substrate.

overlapped patches and gaps between the crystallites were recognized. A total coverage of >90% was estimated for the film at the saturated loading of nanosheets.

By immersion of this substrate with LDH nanosheets in the formamide suspension of oxide nanosheets, they were adhered to the substrate surface via electrostatic attraction force. The AFM image shown in Figure 3b visualizes a dense tiling of $Ti_{0.91}O_2$ nanosheets with a lateral size of several hundred nanometers. The coverage and arrangement of the deposited sheets seem comparable to that of $Ti_{0.91}O_2$ nanosheets assembled with polyelectrolytes, e.g., poly(diallyldimethyl-ammonium chloride),[18a,b] which may be taken as the standard film. $Ca_2Nb_3O_{10}$ nanosheets could also be adsorbed to the surface (Figure 3c). These results indicate the deposition under the conditions above could lead to a substantial coverage with LDH nanosheets and oxide nanosheets in alternating sequence.

The growth of multilayer films composed of LDH nanosheets and oxide nanosheets was followed by UV−visible absorption spectra measured immediately after deposition of each bilayer. The nearly linear increment of absorbance at 260 nm for $Ti_{0.91}O_2$ nanosheet and 190 nm for $Ca_2Nb_3O_{10}$ nanosheet (see Figure 4) clearly demonstrates a successful layer-by-layer assembly between LDH nanosheets and oxide nanosheets. Note that $Mg_{2/3}Al_{1/3}(OH)_2$ nanosheets do not give an appreciable optical absorption in this wavelength range. The absorbance of 1.1 at 260 nm after deposition of 10 bilayers of $Mg_{2/3}Al_{1/3}(OH)_2$/$Ti_{0.91}O_2$ was very similar to that for multilayer films of $Ti_{0.91}O_2$ nanosheet fabricated with polyelectrolytes,[18] suggesting comparable film quality. Similarly, an absorbance of 1.08 was measured for the $(Mg_{2/3}Al_{1/3}(OH)_2/Ca_2Nb_3O_{10})_{10}$ film.

Characterizations of Multilayer Films. XRD data for the obtained films of $(Mg_{2/3}Al_{1/3}(OH)_2/Ti_{0.91}O_2)_n$ exhibited broad peaks centered at a 2θ value of 7.4 and 15.0° (Figure 5a). Their intensity was enhanced progressively with increasing the number of deposition cycles. The diffraction features can be ascribed to the basal series arising from a nanostructure of repeating $Mg_{2/3}Al_{1/3}(OH)_2/Ti_{0.91}O_2$ bilayers. The repeating distance of 1.2 nm can be reasonably accounted for by the sum of the crystallographic thickness of LDH nanosheet, 0.48 nm, and its oxide counterpart, 0.73 nm. AFM data in Figure 3 indicate that alternate stacking of LDH nanosheets and oxide nanosheets was not perfectly ideal. There were overlaps and gaps between the sheets in addition to the dominating monolayer region. Despite these aspects leading to some defects, the evolution of Bragg peaks indicates that the target sandwich layered materials, in which two kinds of nanosheets are directly stacked, were formed as the average structure. The weak intensity may be partly due to disorder in the stacked structure. A fair similarity in X-ray scattering amplitudes of the two kinds of nanosheets may also contribute to it.

In accordance with this discussion, the films of $(Mg_{2/3}Al_{1/3}(OH)_2/Ca_2Nb_3O_{10})_{10}$ exhibited much stronger and better-defined diffraction peaks at 4.2 and 10.2° in 2θ (Figure 5b). Note that $Ca_2Nb_3O_{10}$ is much thicker having a heavy element (Nb) to produce a structure factor in large magnitude. The repeating spacing of 2.0 nm is again close to the sum of the thickness of the constituent nanosheets (0.48 nm for $Mg_{2/3}Al_{1/3}(OH)_2$ and 1.44 nm for $Ca_2Nb_3O_{10}$).

In addition to these diffraction peaks derived from the stacked structures, there was a faint feature at $2\theta = 11.3°$ for both
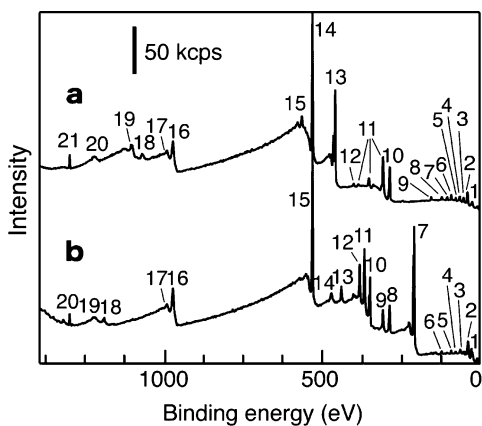
Figure 6. Survey XPS spectra for the multilayer films of (a) $(Mg_{2/3}Al_{1/3}$-$(OH)_2/Ti_{0.91}O_2)_{10}$ and (b) $(Mg_{2/3}Al_{1/3}(OH)_2/Ca_2Nb_3O_{10})_{10}$. Key for (a): (1) O 2s, 23.2 eV; (2) Ti 3p, 37.6 eV; (3) Mg 2p, 50.6 eV; (4) Ti 3s, 63.2 eV; (5) Al 2p, 74.8 eV; (6) Mg 2s, 89.6 eV; (7) Si 2s, 102.4 eV; (8) Al 2s, 120.0 eV; (9) Si 2s, 153.6 eV; (10) C 1s, 284.8 eV; (11) Mg KLL, 307.2, 352.8, 386.4 eV; (12) N 1s, 399.9 eV; (13) Ti $2p_{3/2}$, 458.7 eV, Ti $2p_{1/2}$, 464.5 eV; (14) O 1s, 530.3 eV; (15) Ti 2s, 565.6 eV; (16) O KLL, 975.2 eV; (17) O KLL, 994.4 eV; (18) Ti LMM, 1074 eV; (19) Ti LMM, 1108 eV; (20) C KLL, 1225 eV; (21) Mg 1s, 1304 eV. Key for (b): (1) O 2s, 25.6 eV; (2) Nb 4p, 36.0 eV; (3) Nb 4s, 60.8 eV; (4) Al 2p, 74.8 eV; (5) Mg 2s, 89.6 eV; (6) Al 2s, 120.0 eV; (7) Nb 3d, 206.7 eV; (8) C 1s, 285.0 eV; (9) Mg KLL, 307.6 eV; (10) Ca 2p, 348.0 eV; (11) Nb $3p_{3/2}$, 365.6 eV; (12) Nb $3p_{1/2}$, 381.6 eV; (13) Ca 2s, 438.0 eV; (14) Nb 3s, 472.0 eV; (15) O 1s, 529.7 eV; (16) O KLL, 976.0 eV; (17) O KLL, 998.2 eV; (18) Ca LMM, 1194 eV; (19) C KLL, 1224 eV; (20) Mg 1s, 1304 eV.

combinations as indicated by a broken line in Figure 5. The *d*-value of 0.76 nm suggests the possible presence of LDH in carbonate form in a small amount.[29] The spontaneous deposition of LDH nanosheets trapping CO_3^{2-} ions might have not been perfectly blocked despite the care described above, although the situation was much better than cases without caution.[31]

XPS survey scans were used to identify the composition of the heteroassembled films (Figure 6). The film of $(Mg_{2/3}Al_{1/3}$-$(OH)_2/Ti_{0.91}O_2)_{10}$ exhibited many peaks, which can be assigned to Ti, Mg, Al, O, C, and N from film components as well as Si from the substrate. As to the multilayer film of $(Mg_{2/3}Al_{1/3}(OH)_2/Ca_2Nb_3O_{10})_{10}$, signals derived from Ca and Nb were detected in addition to those from Mg, Al, O, C, and N.

Carbon was found to be mainly present at the very surface by XPS depth analysis (Figure 7); its content drastically dropped to a constant low level after a short sputtering time. Nitrogen was also discerned in a trace level in the analysis. The carbon and nitrogen elements in the inner part of the film may come from remaining formamide and contaminating CO_3^{2-} ions. This can be further proved by FT-IR analysis (Supporting Information, Figure S2).

In the depth analysis, relatively steady plateaus were reached after a sputtering time of 5 min, where the metal contents might be regarded as reflecting the intrinsic chemical composition of the films. Atomic ratios of Mg/Al and Ca/Nb roughly corresponded to the expected values of 2/1 and 2/3 for the constituent nanosheets, respectively, showing the validity of analysis. Ti, Nb, and Al are taken as measures of real compositions, taking into account their high reliability in XPS quantitative analysis. Accordingly, the average molar ratio of LDH nanosheet to oxide nanosheet in the multilayer films was estimated to be 1/1.1 for $(Mg_{2/3}Al_{1/3}(OH)_2/Ti_{0.91}O_2)_{10}$ and 1/0.51 for $(Mg_{2/3}Al_{1/3}(OH)_2/Ca_2Nb_3O_{10})_{10}$, respectively.

Two plausible models involving charge balance and area balance may be theoretically considered for the formation of these inorganic sandwich layered materials composed of the oppositely charged nanosheets. In the charge-balance model, LDH nanosheets and oxide nanosheets are combined in a ratio to attain the charge neutrality for the total system. However, the total areas of LDH nanosheets and oxide sheets deviate from each other due to an intrinsic difference in layer charge density. On the other hand, the area-balance model assumes a mixing ratio, which provides equal area of two kinds of nanosheets in the stacked systems. Some additional counterions, possibly $(C_4H_9)_4N^+$ or protons, are needed for charge compensation. It is important to discuss which model was followed in the real process.

The two-dimensional unit cell of $Ti_{0.91}O_2$ nanosheets, a region encircled by bold lines in Figure 1a, has an area of 0.112 nm^2 ($=0.3760 \times 0.2976$), containing two formula units with a net negative charge of 0.70^-. On the other hand, the unit cell area of $Mg_{2/3}Al_{1/3}(OH)_2$ nanosheets is 0.080 nm^2 ($=0.304^2 \times \sin 120°$) containing a net positive charge of 0.33^+ (Figure 1c). Assuming that the charge balance was followed, the molar ratio of $Mg_{2/3}Al_{1/3}(OH)_2$ to $Ti_{0.91}O_2$ is calculated to be 1/0.95. On the other hand, the area balance should yield a molar ratio of 1/1.43. The molar ratio of $Mg_{2/3}Al_{1/3}(OH)_2$ nanosheets to $Ti_{0.91}O_2$ nanosheets, 1/1.1, determined by XPS analysis above falls just between theoretical values of charge balance and area balance. However, considering the existence of LDH in carbonate form in the sample, a practical content of $Mg_{2/3}Al_{1/3}(OH)_2$ nanosheets combined with $Ti_{0.91}O_2$ nanosheets was less than the measurement. Thus, the effective molar ratio of $Mg_{2/3}Al_{1/3}(OH)_2$ nanosheets to $Ti_{0.91}O_2$ nanosheets may be smaller than 1/1.1, and the yield may be somewhat closer to the theoretical value of area balance.

The unit cell area of $Ca_2Nb_3O_{10}$ nanosheet is 0.149 nm^2 ($=0.3861^2$) containing one negative charge (Figure 1b). In the same way, the ratio of $Mg_{2/3}Al_{1/3}(OH)_2$ to $Ca_2Nb_3O_{10}$ is calculated to be 1/0.33 for the charge balance process and 1/0.54 for the area balance one. The aforementioned molar ratio of $Mg_{2/3}Al_{1/3}(OH)_2$ nanosheets to $Ca_2Nb_3O_{10}$ nanosheets in the obtained film was 1/0.51 when calculated from the content of Al and Nb. As suggested by XRD analysis, there also existed some amount of LDH accommodating CO_3^{2-} ions. If we take out its content, the effective molar ratio should be close to the theoretical value of area balance. Therefore, the area balance model might be more reasonable in the layer-by-layer assembly process. This may be compatible with the AFM data, which indicate alternate and nearly full coverage by LDH nanosheets and their oxide counterparts.

Flocculation into Sandwich Layered Materials. Sandwich-structured materials in powder form were spontaneously formed through a flocculation procedure involving the mixing of the formamide suspensions of LDH nanosheets and oxide nanosheets. Two control experiments were performed to flocculate the oppositely charged nanosheets in a different ratio on the basis of charge balance and area balance. The chemical analysis results of the products are tabulated in Table 1. The mixing on the basis of charge balance yielded molar ratios of LDH nanosheets to oxide nanosheets as 1/0.94 and 1/0.38 for $Ti_{0.91}O_2$ and $Ca_2Nb_3O_{10}$, respectively. These data are both close to the theoretical values of charge balance (1/0.95 for $Ti_{0.91}O_2$ and
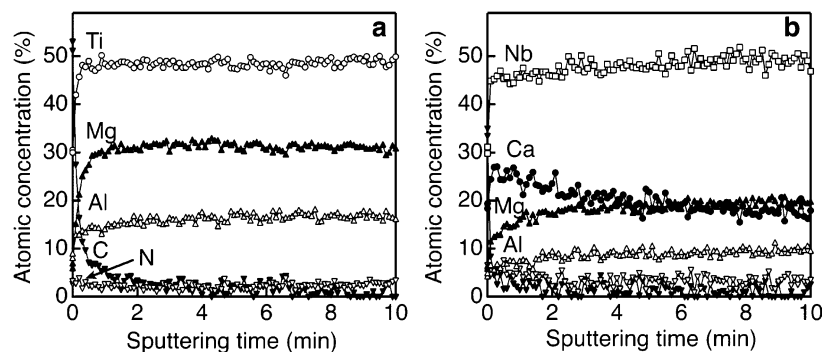
Figure 7. XPS depth profile for the multilayer films of (a) $(Mg_{2/3}Al_{1/3}(OH)_2/Ti_{0.91}O_2)_{10}$ and (b) $(Mg_{2/3}Al_{1/3}(OH)_2/Ca_2Nb_3O_{10})_{10}$. Symbols of open circles, closed circles, open squares, closed triangles, open triangles, closed inverted triangles, and open inverted triangles denote the data for Ti, Ca, Nb, Mg, Al, C, and N, respectively.

Table 1. Chemical Analysis Results of Flocculated Samples

$Mg_{2/3}Al_{1/3}(OH)_2/Ti_{0.91}O_2$				
mixing ratio	Ti (wt %)	Mg (wt %)	Al (wt %)	ratio in product
1/1.43 (area balance)	31.4	8.3	5.2	1/1.25
1/0.95 (charge balance)	31.8	10.7	7.0	1/0.94

$Mg_{2/3}Al_{1/3}(OH)_2/Ca_2Nb_3O_{10}$					
mixing ratio	Ca (wt %)	Nb (wt %)	Mg (wt %)	Al (wt %)	ratio in product
1/0.54 (area balance)	9.7	40.6	4.1	2.3	1/0.57
1/0.33 (charge balance)	10.4	37.4	5.2	3.2	1/0.38

1/0.33 for $Ca_2Nb_3O_{10}$). As to the experiments based on area balance (1/1.43 for $Ti_{0.91}O_2$ and 1/0.54 for $Ca_2Nb_3O_{10}$), flocculation also took place instantly upon mixing. The chemical analysis results produced a molar ratio of LDH nanosheets to oxide nanosheets, 1/1.25 for $Ti_{0.91}O_2$ and 1/0.57 for $Ca_2Nb_3O_{10}$, respectively, being close to the initial mixing ratios. All these results suggest that flocculation proceeds flexibly according to the initial ratio. Some additional counterions may be trapped to neutralize the excessive charge. On the basis of XRD data as will be presented below, the amount of LDH in carbonate form as a side product seemed trivial in the flocculated products when compared with the layer-by-layer assembled films. A relatively shorter time in the flocculation process may be responsible for this aspect because the exposing time to CO_2 containing atmosphere was limited.

XRD patterns of the flocculated products of $Mg_{2/3}Al_{1/3}(OH)_2/Ti_{0.91}O_2$ and $Mg_{2/3}Al_{1/3}(OH)_2/Ca_2Nb_3O_{10}$ showed two basal peaks indicated by triangle (Figure 8). No noticeable difference was observed for samples prepared on the basis of charge balance and area balance. The repeating basal distance values of 1.2 and 2.0 nm were exactly the same as those of the multilayer films, being again well-consistent with the sum of crystallographic thickness of LDH nanosheets and oxide nanosheets. The peaks were stronger than those for the films, which may be explained in terms of a larger number of the stacked nanosheets. Additional reflection peaks were also observed in a higher 2θ range. A peak at $2\theta = 60.8°$ (indicated by a square) can be assigned as intrasheet 11 reflection of hexagonal LDH structure. On the other hand, two peaks at $2\theta = 48.5$ and $62.6°$ (indicated by circles) for the $Mg_{2/3}Al_{1/3}(OH)_2/Ti_{0.91}O_2$ system are 20 and 02 peaks arising from the rectangular architecture of $Ti_{0.91}O_2$ nanosheet. Similarly, five peaks at $2\theta = 23.1, 32.9, 47.2, 53.1,$ and $68.8°$ for the $Mg_{2/3}Al_{1/3}(OH)_2/Ca_2Nb_3O_{10}$ sample can be readily assigned as 10, 11, 20, 21,

and 22 intrasheet reflections from a square lattice of $Ca_2Nb_3O_{10}$ nanosheet. The presence of these reflections indicates that the two-dimensional structures of LDH nanosheet and oxide counterparts remained practically unchanged in the process.[32]

These intrasheet reflections had an anisotropic profile having a tail toward a higher angle side, suggesting irregular sheet-to-sheet registry. In addition, broad humps appearing at $20-40°$ in 2θ for $Mg_{2/3}Al_{1/3}(OH)_2/Ti_{0.91}O_2$ and $25-35+$ and $55-60°$ for $Mg_{2/3}Al_{1/3}(OH)_2/Ca_2Nb_3O_{10}$ may be also associated with such disordered structures. Similar diffraction features have been found in flocculates prepared by restacking nanosheets with various ionic species.[33,34] The turbostratic structure may be reasonable taking into account the synthetic process involving spontaneous room-temperature combination of oppositely charged nanosheets in liquid phase.

TEM observations also provided direct evidence for the formation of sandwich structures. Two kinds of nanosheets, visualized as darker contrast fringes with a different thickness, could be resolved in the TEM image of the $Mg_{2/3}Al_{1/3}(OH)_2/Ti_{0.91}O_2$ sample (Figure 9a). The lamellar fringe was not completely parallel but slightly twisted in some areas, which may be due to high flexibility of the nanosheets.[35−37] The bilayer thickness of 1.2 nm corresponds to the sum of the thickness of the two constituent nanosheets. In Figure 9b, the darker contrast line refers to the octahedral slab of $Ca_2Nb_3O_{10}$ nanosheets. The $Ca_2Nb_3O_{10}$ unit contains three such octahedral slabs along the sheet normal in equidistance, which was clearly seen in the image. There existed another layer with a weaker contrast in the gallery of two neighboring $Ca_2Nb_3O_{10}$ units. Its thickness of ~0.5 nm is similar to the thickness of $Mg_{2/3}Al_{1/3}(OH)_2$ nanosheets (0.48 nm). Selected-area electron diffraction patterns taken with electron beam perpendicular to the stacked layer were composed of sets of diffraction rings attributable to constituent nanosheets (see Supporting Information, Figure S3), indicating again intactness of nanosheets after flocculation.

There is a unique class of so-called mixed layered materials, in which two different host layers are stacked. Such most typical

(32) The absence of intrasheet reflections in the film samples can be explained by preferential orientation of stacked nanosheets having their normal perpendicular with respect to a substrate.
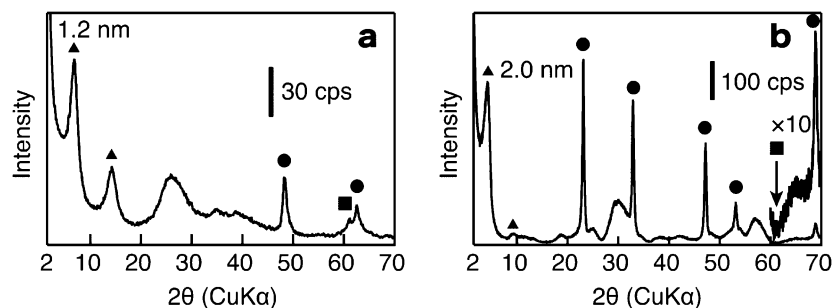(33) Xin, H.; Ma, R.; Wang, L. Z.; Ebina, Y.; Takada, K.; Sasaki, T. *Appl. Phys. Lett.* **2004**, *85*, 4187.
(34) Ebina, Y.; Sasaki, T.; Harada, M.; Watanabe, M. *Chem. Mater.* **2002**, *14*, 4390.
(35) Wang, L. Z.; Sasaki, T.; Ebina, Y.; Kurashima, K.; Watanabe, M. *Chem. Mater.* **2002**, *14*, 4827.
(36) Ma, R.; Bando, Y.; Sasaki, T. *J. Phys. Chem. B* **2004**, *108*, 2115.
(37) Li, L.; Ma, R.; Ebina, Y.; Iyi, N.; Ebina, Y.; Takada, K.; Sasaki, T. *Chem. Commun.* **2006**, 3125.

Figure 8. XRD patterns of the flocculated samples of (a) $Mg_{2/3}Al_{1/3}(OH)_2/Ti_{0.91}O_2$ and (b) $Mg_{2/3}Al_{1/3}(OH)_2/Ca_2Nb_3O_{10}$. The mixing molar ratio of LDH nanosheets to oxide nanosheets is 1/1.43 for (a) and 1/0.54 for (b). Symbols of triangles, circles, and squares denote basal peaks and intrasheet reflections from oxide nanosheets and LDH nanosheets, respectively.
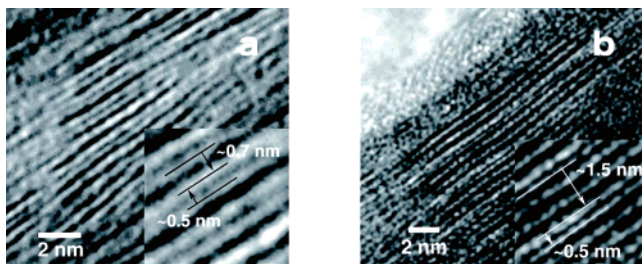
Figure 9. High-resolution TEM images of flocculated materials of (a) $Mg_{2/3}Al_{1/3}(OH)_2/Ti_{0.91}O_2$ and (b) $Mg_{2/3}Al_{1/3}(OH)_2/Ca_2Nb_3O_{10}$.

examples are interstratified clay minerals,[38] which have been investigated from mineralogical and structural viewpoints. In these structures, different kinds of clay aluminosilicate sheets, in different composition but usually with the same structure and electric charge, are stacked accommodating countercations between them.

In contrast to these rather usual mixed layered materials, there is, although limited in abundance, a family of naturally occurring clay minerals called chlorite,[39] which is composed of a positively charged LDH-like layer and a negatively charged aluminoslicate layer. Synthetic materials with a structure comparable to that of chlorite have also been reported. Their synthesis involved titration of layered hosts with an alkali solution to form metal hydroxide layers (e.g., $Ni(OH)_2$) in-situ, in the interlayer

space.[40,41] The sandwich layered materials in this study are similar to these materials in that two oppositely charged layers are stacked in an alternating fashion. The exfoliation—restacking process can allow artificial and rational combinations of various nanosheets with different compositions and atomic architectures.

Conclusions

We have demonstrated the successful fabrication of a new type of inorganic sandwich structured materials via layer-by-layer self-assembly and spontaneous flocculation between positively charged LDH nanosheets and negatively charged oxide nanosheets. The characterizations revealed the layered structures, in which LDH nanosheets and oxide sheets were alternately stacked. Other negatively charged nanosheets, e.g., MnO_2, etc., may also be used to construct similar inorganic sandwich lamellar materials with LDH nanosheets to design the desired functionality for various applications.

Supporting Information Available: In-plane XRD data for monolayer films of nanosheets, FT-IR absorption spectra of films of LDH/oxide nanosheets, and selected area electron diffraction data for flocculated samples of LDH/oxide nanosheets. This material is available free of charge via the Internet at http://pubs.acs.org.

JA0719172

(38) Reynolds, R. C. *Interstratified Clay Minerals;* In *Crystal Structures of Clay Minerals and Their X-ray Identification*; Brindley, G. W., Brown, G., Eds.; Mineralogical Society: London, 1980.
(39) Bailey, S. W. Chlorites: Structure and Crystal Chemistry. In *Hydrous Phyllosilicates*; Bailey, S. W., Ed.; Mineralogical Society of America: Chelsea, MI, 1988; Vol. 19, pp 347–403.
(40) (a) Yamanaka, S.; Brindley, G. W. *Clays Clay Miner.* **1978**, *26*, 21. (b) Ohtsuka, K.; Suda, M.; Tsunoda, M.; Ono, M. *Chem. Mater.* **1990**, *2*, 511.
(41) (a) Feng, Q.; Honbu, C.; Yanagisawa, K.; Yamasaki, N.; Komarneni, S. *J. Mater. Chem.* **2000**, *10*, 483. (b) Xu, Y.; Feng, Q.; Kajiyoshi, K.; Yanagisawa, K. *Chem. Mater.* **2002**, *14*, 697.